Near Magnetic Field Emission Analysis for IGBT and SiC Power Modules

Boyi Zhang, Hui Zhao and Shuo Wang
Power Electronics and Electrical Power Research Lab
University of Florida, Gainesville, FL 32611
Email: shuowang@ieee.org; zby0070@ufl.edu

***Abstract*—Power modules with high-speed power devices such as IGBTs and SiC MOSFETs have become crucial components of medium to high power applications. However, their faster switching speed and compact design raise near magnetic field emission issues. The near magnetic field from the high-speed power modules could contaminate the peripheral circuits and filters. In this paper, the near magnetic field emission is analyzed for three power modules. The root cause and sources of the near magnetic emission are identified. Based on the analysis, the near magnetic field is predicted and verified with finite element analysis (FEA) simulation and measurement.**

***Index Terms*— Near magnetic field, power module, bus bar, electromagnetic interference.**

I. Introduction

Power modules with high-speed power devices such as IGBTs and SiC MOSFETs have become a crucial part of medium to high power applications such as electric vehicles and aviation. The fast switching speed enabled by IGBTs and SiC MOSFETs reduces the switching loss [1]. As a result, the efficiency of the power electronics system is increased. With higher efficiency, the power electronics system could apply compact design to increase power density. In compact designs, peripheral circuits, and passive components, including drivers and filters, are very close to the power module [2]. Because of the close distance, the near magnetic field generated by the switching of power modules could couple to the peripheral circuit and filters. The near field coupling degrades the performance of EMI filters [3], leading to high EMI noise in the system. The near magnetic field generated by the power module could also induce noises in the circuits such as driver board and active filters. Because voltage and current in the power modules are much larger than the ones in drivers and active filters, a small portion of coupling could cause significant damage [4]. As a result, it is crucial to investigate the near magnetic field emission of power modules.

Exiting research on the field emission of power electronics includes both near and far-field emissions. The emission from components, such as inductors [3] [4], plate capacitors [6], and microstrips [7], was investigated. At the PCB level [8], only the far-field emission is evaluated. The near magnetic field is measured in [9] for a low power module with one switching device. The near field emission from a multi-chip power module was measured in [10]. The near magnetic field of a buck converter circuit is modeled with a simple geometry model in [11]. The near field analysis in these papers mainly focused on the near magnetic field emits from the traces of the power module. However, in high power applications, the bus bars are usually integrated inside the power module. The large dimension of bus bars changes the current distribution in the system [5] and shift the near magnetic field patterns. The far-field radiation of power electronics systems is studied in [12] – [14]. The far-field radiation from the power electronics system is caused by the common-mode current in the input and output cables. The cables are modeled as unintentional antennas in [12]. The radiation is measured with antennas at a far distance (> 1m) from the system. The interaction between the power module and the peripheral circuit, on the other hand, is in very close distance (<30 mm). As a result, near field analysis should be considered.

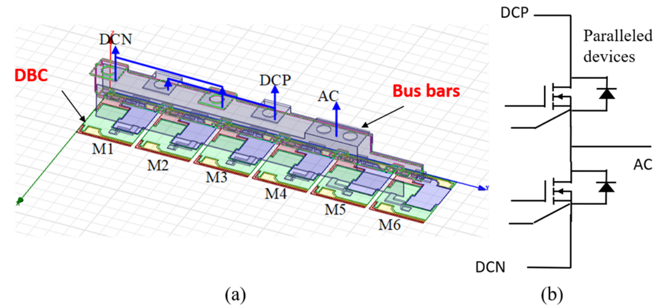

Fig. 1. Power module package structure (a) A power module package with DBC and bus bars (b) the circuit schematic of the power module

In this paper, the near magnetic field emission is analyzed for power modules with two different busbar structures. The root cause of near magnetic field emission and major emission sources are identified. Simulations are conducted in FEA software. The simulation and experiments are compared. Based on the analysis, guidelines are provided on how to design the power electronics system with power modules to reduce the interference from the near magnetic field emission.

II. Noise current analysis and emission source identification

To analysis the near magnetic field, it is important to identify the root cause. Based on electromagnetic theory, the cause of near magnetic field is generated by current loops. Therefore, identifying the current and the geometries that carry the current is essential.

As shown in Fig.1, there are two major parts inside the power module package: the bus bars and direct bond copper (DBC). The bus bars are used for the connection between the power module and outside circuit, including the DC source and load. The positive (DCP) terminal and negative (DCN) terminal are connected to the DC power source. AC terminal is connected to

the load. The DBC of the power module is used for the connection inside the power module, including the connection between the power device dies and the connection between the power device and the bus bars. The DBC and wire bond connections are usually insulated with silicone gel. Therefore, the power semiconductor chips can be very close to each other. The bus bars are insulated with air. As a result, the clearance between the DCP and DCN terminals must be larger than the chips and traces on the DBC. In addition, the bus bars also need to carry a large current, the heat on the busbar generated by the current need to dissipate through the air. The DBC, on the other hand, has a ceramic and a metal layer on the bottom. The thermal resistance of the DBC is smaller than the bus bars. For both clearance and thermal reasons, bus bars have much larger dimensions compared to DBC.

In most applications, the switching frequency of power semiconductor devices is much higher than the load current frequency. Therefore, the load current and DC supply voltage are considered as constant during the switching transient of power devices. The near magnetic field emission is generated by the current loops. From the EMI perspective, the interference noise is caused by the high-frequency components of the near magnetic field. During the switching process, the current in the power loop of the power module changes drastically. High *di/dt* generates wideband EMI noise. As a result, the high-frequency components of the near magnetic field are caused by the EMI noise current inside the power module.

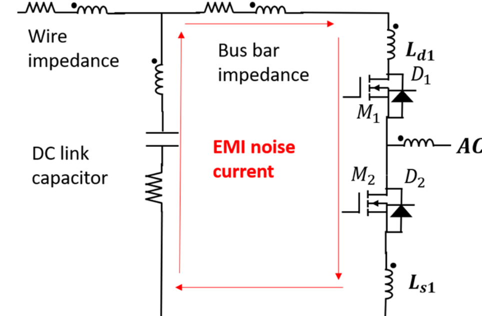

Fig. 2. EMI NOISE current in the power loop of a half-bridge power module

During the switching transient of power semiconductor devices, because large current and di/dt, the voltage would be induced on the parasitic inductance. The magnetic energy stored in the parasitic inductance along with the electric charge stored in the junction capacitance of power devices resonant in the power loop [2]. It causes large and wideband EMI noise currents. As shown in Fig. 2. This EMI noise current flows between the positive and negative terminals. Therefore, the current flows through the bus bars and the DBC. The magnitude of this EMI noise current depends on the initial condition of parasitic inductance and junction capacitance. Large parasitic inductance and junction capacitance will result in large EMI noise current, hence large near magnetic field emission. In addition, the near magnetic field depends on the current loop size as well as the current value. A large current loop area leads to large near magnetic field emission [4].

The bus bars in power modules have different types of structures. For power modules made with DBC and wire bond packaging technology, the structures of bus bars can be divided into two kinds: the vertical structure and horizontal structure. The bus bars and the current loops formed by the bus bars are shown in Figs. 3 – 5. In this paper, three power modules are presented and discussed.

An intelligent IGBT power module (IPM) 2MBI1400VXB-120P-50 is shown in Fig. 3 (a), the IGBT power module has vertical busbars. There are six cells M1-M6 evenly distributed at the bottom of the module. The whole 3D model is shown in Fig. 1 (a). The inner structure of the IPM is shown in Fig. 3 (b). Fig.3 (c) shows the 3D model for one cell. It has four IGBTs and four diodes. The IPM has 12 IGBTs and 12 diodes on top and 12 IGBTs and 12 diodes on the bottom in total.

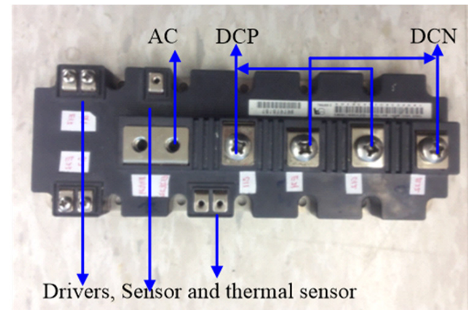

(a)

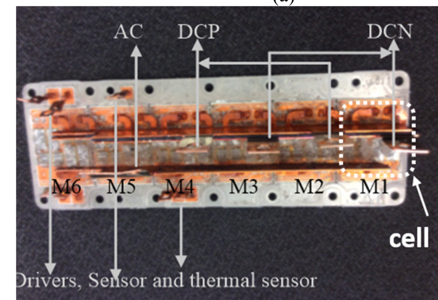

(b)

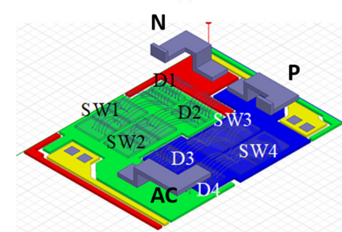

(c)

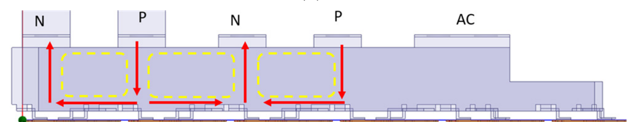

(d)

Fig. 3. IPM structure and current loops. (a) IPM overview (b) inner structure of the IPM (c) detailed structure of one cell and (d) EMI noise current paths (red arrow) and equivalent current loops (yellow dash line) on the bus bars.

The EMI noise current paths on the bus bars are shown in Fig. 3 (d). The red arrows show the EMI noise current from P terminals to N terminals. The yellow dash line shows the equivalent current loops. Because of the large loop area and large current, the equivalent current loops in Fig. 3 (d) generates a large near magnetic field. It can be predicted that the near magnetic field emission of this IPM is mainly caused by these current loops.

Fig 4 shows a multi-chip power module (MPM) with SiC MOSFETs and SiC Schottky diodes (SBD). The MPM is a half-bridge module. Each switch has six SiC MOSFETs and six SiC Schottky diodes in parallel. The inner stricture of the MPM is shown in Fig. 4 (b). The EMI NOISE current path and equivalent loops are shown in Fig.4 (c). The bus bar structure in this power module is also vertical. Similar to the IPM, the large loop area formed by the bus bars generates large near magnetic field emission to the side of the power module.

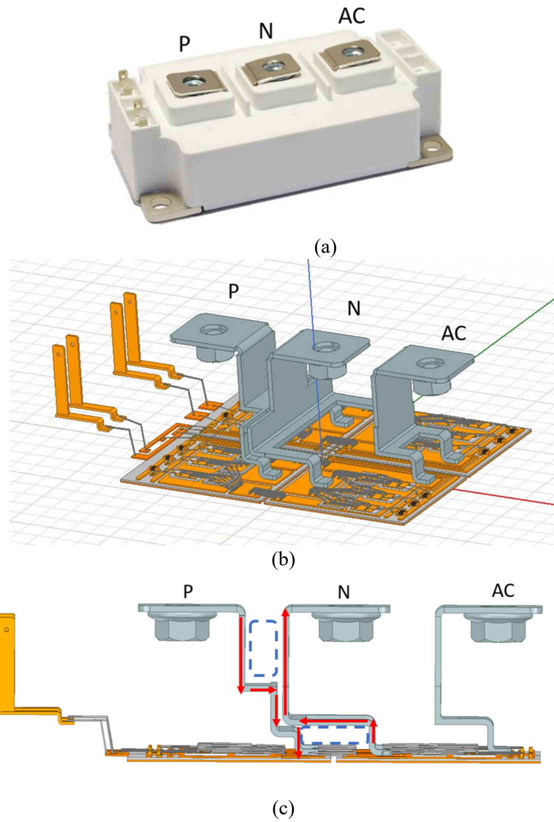

Fig. 4. SiC MPM structure and current loops. (a) Module overview (b) inner structure (c) EMI noise current paths (red arrow) and equivalent current loops (blue dash line) on the bus bars.

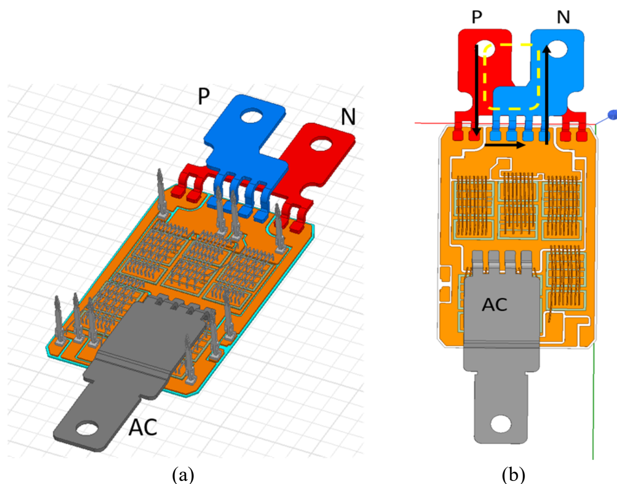

Fig. 5. A phase-leg of an IGBT three-phase inverter (a) inner structure and (b) EMI noise current path (black arrow) and equivalent current loop (yellow dash line) on bus bars

Fig.5 shows the package structure inside one phase leg of an IGBT three-phase inverter. The other two phase-legs have the exact same structures as Fig.5 (a). The Bus bars in Fig. 5 (a) has the horizontal structure. The power module is connected to the DC source, and load from the side of the module instead of the top. The EMI noise current paths are shown in Fig. 5 (b). Different from the vertical bus bar structures, the near magnetic field emission of the horizontal structure is in the vertical (Z) direction. The near field is more likely to couple the circuit on the top of the power module.

Based on the analysis in this Section, three conclusions can be made: 1. The near magnetic field of power module is generated by the EMI noise current in the power loop. 2. The major sources of emission are the current loops formed by the bus bar of the power module. 3. For the vertical bus bar structure, the near field emission on the side of the power module is the largest. For the horizontal bus bar structure, the near field emission on the top will be the largest.

III. Near Magnetic Field Emission Simulation and Experiments

The near magnetic field of power modules is simulated in FEA software to verify the analysis in Section II. The experiment with the same setup with the simulation is conducted to verify the analysis as well as the simulation result. The simulations are carried out in three steps. Parasitic parameter extraction, circuit simulation, and field simulation.

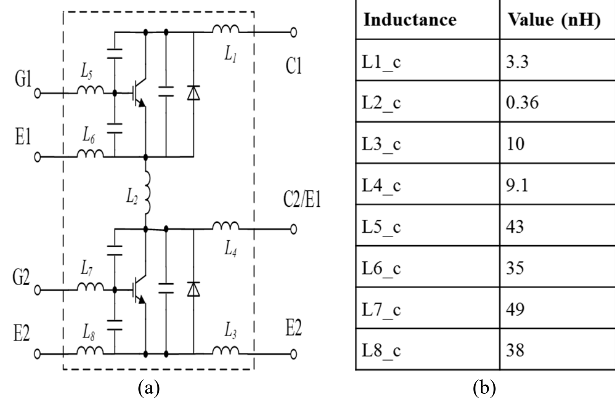

Inductance	Value (nH)
L1_c	3.3
L2_c	0.36
L3_c	10
L4_c	9.1
L5_c	43
L6_c	35
L7_c	49
L8_c	38

Fig. 6. (a) Equivalent circuit of the IPM with parasitic parameters and the extracted parasitic parameters.

A. Parasitic parameter extraction

The equivalent circuit of a half-bridge power module with parasitic parameters is shown in Fig. 6 (a). The parasitic inductance and junction capacitance inside the power module determine the magnitude and frequency of the EMI noise current inside the power loop. As a result, to correctly model the near magnetic field emission, the parasitic parameters of the power module need to be extracted. In this paper, the parasitic parameters are extracted with Ansys Q3D. The self and mutual inductance of each parallel cell are extracted with the same technique in [2]. Although it is the parasitic inductance in the power loop that determines the EMI noise current, the parasitic inductance in the drive loop is also important. Because it determines the switching waveforms of the power semiconductor devices. Therefore, the parasitic inductance of

both the power loop and drive loop is extracted, as shown in Fig. 6 (b).

B. Circuit simulation

The extracted parasitic parameters of both the power loop and drive loop are then imported to Ansys Simplorer for circuit simulation. As shown in Fig. 7, the power semiconductors are modeled with the device characterization tool of the Ansys Simplorer. In this way, the voltage and current inside the power module power loops can be simulated.

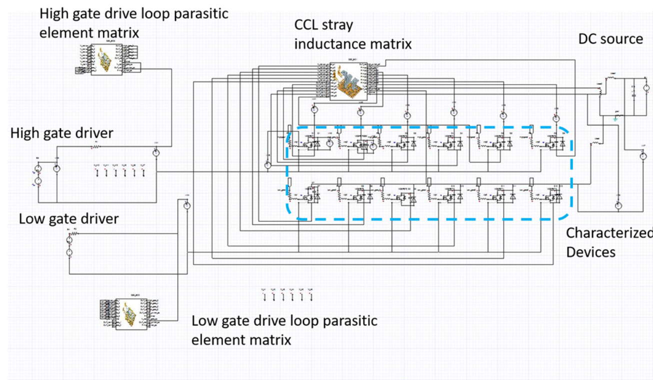

Fig. 7. Circuit simulation with extracted parasitic parameters.

C. Field simulation

After the voltage and current of the drain to source terminals of the switching devices are simulated, voltage and current sources are added to the device die structure in the 3D model. Based on the substitution theory, the simulation has the same output by substituting the device dies with voltage and current sources. Because the current inside the power loop is the same as the one in the real application, the near field simulation could provide a good prediction.

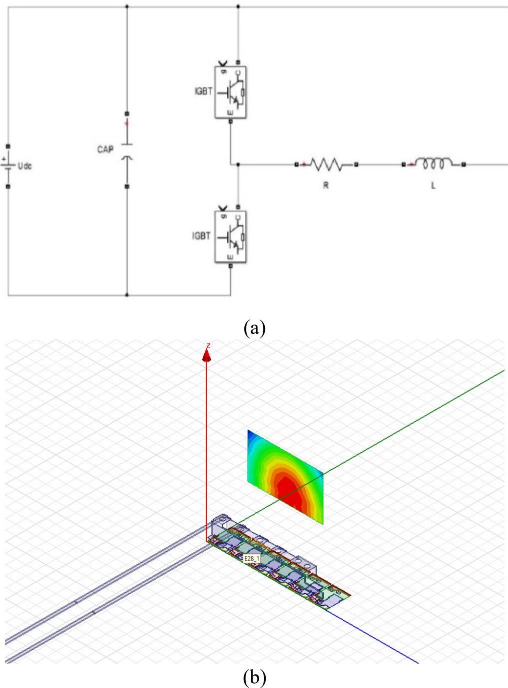

(a)

(b)

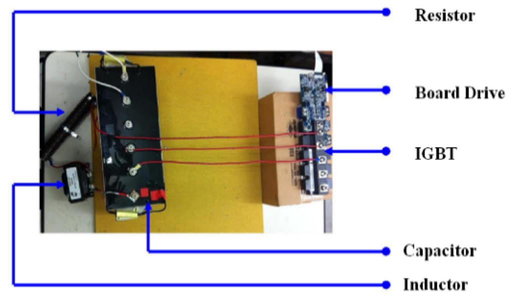

(c)

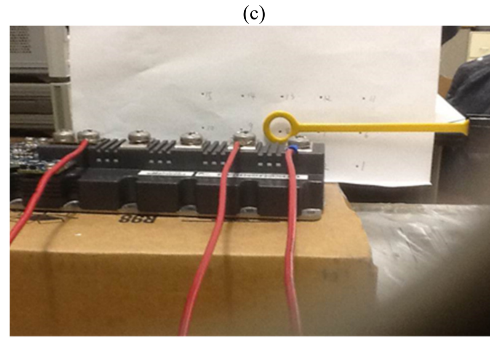

(d)

Fig. 8. The setup for the simulation and experiment. (a) a simplified circuit schematic, (b) Simulation setup, and (c) experiment set up and (d) near field probe and the plane of measurement.

The simulation and experiment are based on a 1000W setup. The load resistor is 10 ohm. The load inductance is 2 mH. DC link voltage is 200V, duty circle is 0.5, and the switching frequency is 1 kHz. Fig. 8 (b) shows the simulation setup for the IPM in Fig. 3. The DC capacitance, inductance, resistance, and the DC power source are placed far (0.5m) away from the IGBT so that their near field emission would not influence the measurement of the emission of the IPM. The wires that connect the DC source and bus bars are set to be parallel and at a constant height. As a result, the near magnetic field generated by the wires is mostly in a vertical direction. The near magnetic field generated by the power module; on the other hand, is mostly in the horizontal direction. Therefore, the wires have little influence on the accuracy of the near magnetic field measurement.

The same simulation setup is used for all three power modules in Figs. 3 – 5. Fig. 9 shows the near magnetic field vectors for the SiC MPM. The magnetic field vector clears shows that the current loops formed by the bus bar are the main source of emission. At the same time, it can be observed that the peripheral of the power module is more severely influenced by the near magnetic field emission than the top.

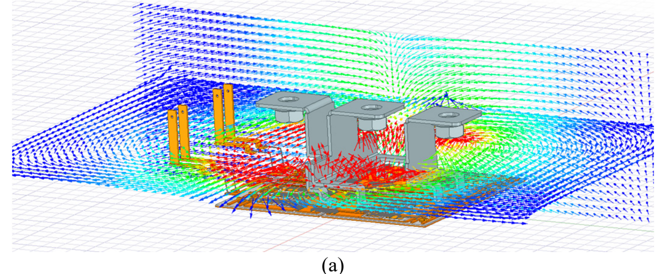

(a)

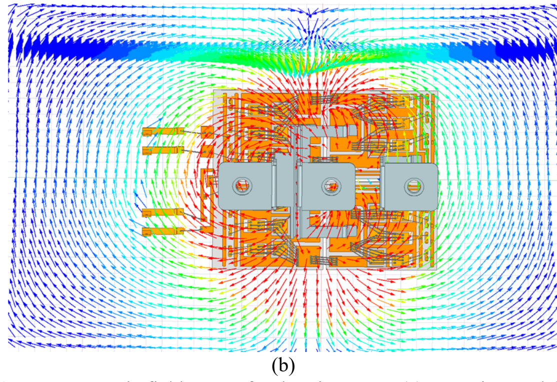

(b)

Fig. 9. Near magnetic field vector for the SiC MPM. (a) Overview and (b) top view.

Fig. 10 shows the near magnetic field vectors of the power module with horizontal busbars. The near magnetic field is concentrated around the bus bars of the module. The major emission is in the Z direction. The near field emission on top of the power module bus bar is the most serious.

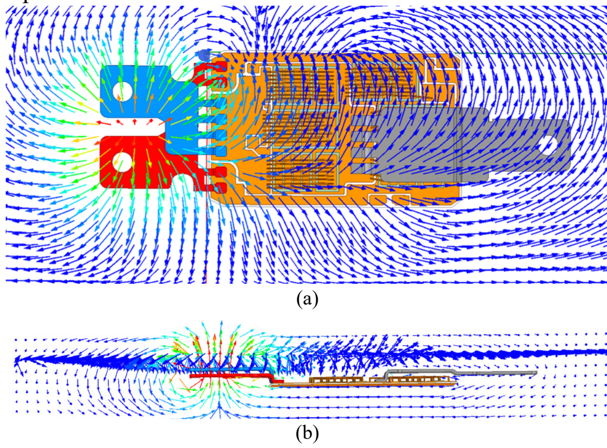

(a)

(b)

Fig. 10. Near magnetic field vectors for a phase leg of the three-phase inverter power module. (a) top view and (b) side view.

D. Experiment

The measurement was conducted with a Beehive Electronics 100-C EMC probe, a coordinate plane, and an Agilent 4395A spectrum analyzer, as shown in Fig. 8 (d). The coordinate had a dimension of 200 mm × 100 mm with an 11×6, 20 mm spaced grid. The distance between the IPM and the coordinate plane is 15 mm. For each grid point on the plane, the EMC probe was placed in the x, y, and z directions to measure the amplitude of the magnetic field $|\boldsymbol{B}_x|$, $|\boldsymbol{B}_y|$ and $|\boldsymbol{B}_z|$ respectively. The amplitude of the total magnetic field strength $\boldsymbol{B}_{Total}$ is calculated by (1) as:

$$|B_{Total}| = \sqrt{|B_x|^2 + |B_y|^2 + |B_z|^2} \quad (1)$$

The comparison between the simulation and experiment is shown in Fig. 11. The results show that the simulated magnetic field distribution can match the measured magnetic field distribution. The difference between the simulated results and the measured result is under 20% within the whole space range.

Only two of the four bus bar terminals are connected to the DC source in the experiment for the IPM to illustrate the effect of unbalanced current. As shown in Fig. 12, because of the proximity effect, the current density on the DC bus bar is not even. As a result, the near magnetic field emission is also not even. The emission is high adjacent to the bus bar terminals with the wire connection.

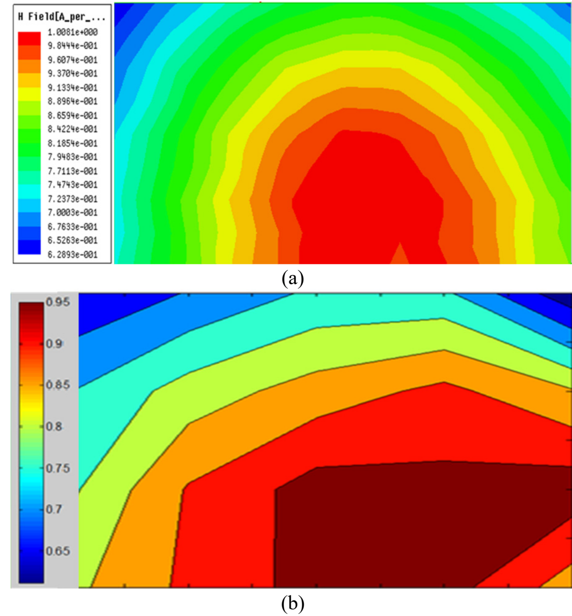

(a)

(b)

Fig. 11. Near magnetic field flux density of the IPM. (a) Simulation and (b) measurement.

E. Discussion

Based on the analysis in this paper, there are several ways to mitigate the influence of the near magnetic field emission.

Firstly, interleaving the bus bar positive and negative terminals could reduce the near magnetic field emission. This is because by interleaving the positive and negative terminals, the current loops formed by the bus bar would have opposite winding directions. As a result, the magnetic field generated by these current loops can cancel each other, resulting in smaller near magnetic field emission.

Secondly, dynamic current balancing is important to reduce the near magnetic field emission. As shown in Fig. 12, the dynamic current could concentrate on a certain part of busbars, leading to a large near magnetic field emission. To balance the dynamic current among the paralleled devices, the layout of the power module should be symmetrical. Other methods, including distributed gate resistors, could also be used. In another simulation, the current in the IPM is balanced using gate resistor methods to show the effect of current balancing. The comparison of the near magnetic field emission is shown in Fig. 13. A reduction can be observed in both magnitude and high emission area.

Thirdly, the near magnetic field emission from vertical and horizontal bus bar structures are different. As a result, to mitigate the influence of the near field emission, sensitive circuits and components should avoid the high emission region like the red zoned in Figs. 4 and 5. If the circuits or components must be placed near the power module, the circuit layout should be designed based on the direction of the magnetic field. Some winding techniques that could reduce the induced noise in the presence of near magnetic field have been proposed in [3] and [15]. Shielding techniques could also be applied to the sensitive

circuit.

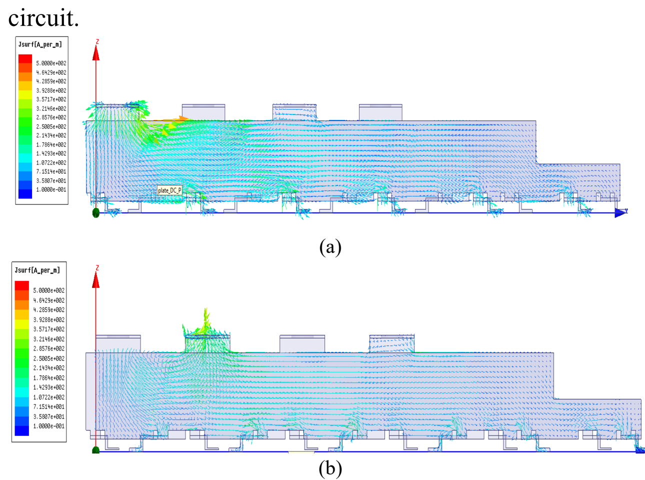
(a)
(b)
Fig. 12. Current distribution on the bus bars. (a) Positive terminal bus bar and (b) Negative terminal bus bar.

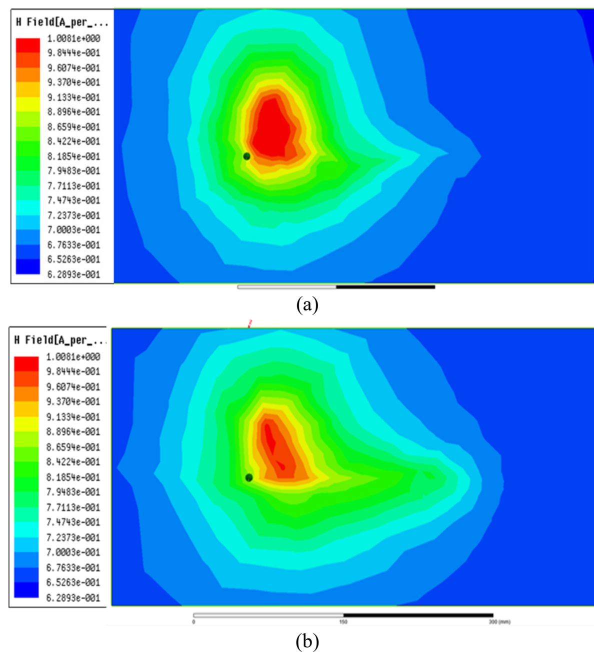

(a)
(b)
Fig. 13. Current distribution on the bus bars. (a) Positive terminal bus bar and (b) Negative terminal bus bar.

IV. Conclusion

In this paper, the near magnetic field emission of the power module is analyzed. Based on the analysis, the EMI NOISE current in the power loop is the root cause of the emission. The current loops formed by the bus bars of the power module are the major source of the near magnetic field emission. FEA simulation and experiments are carried out the verify the simulation. A good agreement is achieved among the analysis, the simulation, and the experiment. Based on the analysis, several techniques that could reduce the near magnetic field emission are discussed.

References

[1] B. Zhang and S. Wang, "A Survey of EMI Research in Power Electronics Systems With Wide-Bandgap Semiconductor Devices," in IEEE Journal of Emerging and Selected Topics in Power Electronics, vol. 8, no. 1, pp. 626-643, March 2020,

[2] B. Zhang and S. Wang, "Parasitic Inductance Modeling and Reduction for a Wire Bonded Half Bridge SiC MOSFET Multichip Power Module," 2019 IEEE Applied Power Electronics Conference and Exposition (APEC), Anaheim, CA, USA, 2019, pp. 656-663

[3] C. Yongbin, S. Wang, Z. Ning, and F. Dianbo, "A Common Mode Inductor With External Magnetic Field Immunity, Low-Magnetic Field Emission, and High-Differential Mode Inductance," Power Electronics, IEEE Transactions on, vol. 30, pp. 6684-6694, 2015.

[4] B. Zhang and S. Wang, "Analysis and Reduction of the Near Magnetic Field Emission From Toroidal Inductors," in IEEE Transactions on Power Electronics, vol. 35, no. 6, pp. 6251-6268, June 2020

[5] N. Zhang, S. Wang and H. Zhao, "Develop Parasitic Inductance Model for the Planar Busbar of an IGBT H Bridge in a Power Inverter," in *IEEE Transactions on Power Electronics*, vol. 30, no. 12, pp. 6924-6933, Dec. 2015.

[6] M. Leone, "The emission of a rectangular power-bus structure at multiple cavity-mode resonances," Electromagnetic Compatibility, IEEE Transactions on, vol. 45, pp. 486-492, 2003.

[7] X. Jun and S. Wang, "Investigating a Guard Trace Ring to Suppress the Crosstalk due to a Clock Trace on a Power Electronics DSP Control Board," Electromagnetic Compatibility, IEEE Transactions on, vol. 57, pp. 546-554, 2015.

[8] J. R. Regue, M. Ribo, J. M. Garrell, and A. Martin, "A genetic algorithm based method for source identification and far-field radiated emissions prediction from near-field measurements for PCB characterization," Electromagnetic Compatibility, IEEE Transactions on, vol. 43, pp. 520-530, 2001

[9] G. Vine, P. Vidal and J. Dienot, "Characterization Method of Radiated Magnetic Field Based on Integrated Antenna Measurement Applied to Power Module Technologies," in IEEE Transactions on Power Electronics, vol. 35, no. 2, pp. 1440-1449, Feb. 2020, doi: 10.1109/TPEL.2019.2916261.

[10] M. Wang, F. Luo and L. Xu, "A Double-End Sourced Wire-Bonded Multichip SiC MOSFET Power Module With Improved Dynamic Current Sharing," in IEEE Journal of Emerging and Selected Topics in Power Electronics, vol. 5, no. 4, pp. 1828-1836, Dec. 2017, doi: 10.1109/JESTPE.2017.2720731.

[11] A. I. Emon, B. Narayanasamy, T. M. Evans, F. Luo and H. A. Mantooth, "Modeling and Analysis of Near-Field Radiated Emission in Wide Bandgap Power Modules," 2019 International Symposium on Electromagnetic Compatibility - EMC EUROPE, Barcelona, Spain, 2019, pp. 333-338, doi: 10.1109/EMCEurope.2019.8871481.

[12] Y. Zhang, S. Wang and Y. Chu, "Investigation of Radiated Electromagnetic Interference for an Isolated High-Frequency DC–DC Power Converter With Power Cables," in IEEE Transactions on Power Electronics, vol. 34, no. 10, pp. 9632-9643, Oct. 2019, doi: 10.1109/TPEL.2019.2892706.

[13] Y. Zhang, S. Wang and Y. Chu, "Analysis and Comparison of the Radiated Electromagnetic Interference Generated by Power Converters With Si MOSFETs and GaN HEMTs," in IEEE Transactions on Power Electronics, vol. 35, no. 8, pp. 8050-8062, Aug. 2020, doi: 10.1109/TPEL.2020.2972342.

[14] J. Yao, S. Wang and H. Zhao, "Measurement Techniques of Common Mode Currents, Voltages, and Impedances in a Flyback Converter for Radiated EMI Diagnosis," in IEEE Transactions on Electromagnetic Compatibility, vol. 61, no. 6, pp. 1997-2005, Dec. 2019, doi: 10.1109/TEMC.2019.2953925.

[15] Y. Lai, S. Wang and B. Zhang, "Investigation of Magnetic Field Immunity and Near Magnetic Field Reduction for the Inductors in High Power Density Design," in IEEE Transactions on Power Electronics, vol. 34, no. 6, pp. 5340-5351, June 2019.

[16] F. C. Lee, J. D. van Wyk, Z. X. Liang, R. Chen, S. Wang and B. Lu, "An integrated power electronics modular approach: concept and implementation," *The 4th International Power Electronics and Motion Control Conference, 2004. IPEMC 2004.*, Xi'an, 2004, pp. 1-13 Vol.1.

[17] F. C. Lee, M. Xu, S. Wang and B. Lu, "Design Challenges For Distributed Power Systems," *2006 CES/IEEE 5th International Power Electronics and Motion Control Conference*, Shanghai, 2006, pp. 1-15.

[18] S. Wang and F. C. Lee, "Investigation of the Transformation Between Differential-Mode and Common-Mode Noises in an EMI Filter Due to Unbalance," in *IEEE Transactions on Electromagnetic Compatibility*, vol. 52, no. 3, pp. 578-587, Aug. 2010.